PAPER Special Section on Microwave and Millimeter-Wave Technologies

Load-Independent Class-E Design with Load Adjustment Circuit Inverter Considering External Quality Factor

Akihiko ISHIWATA[†a)], **Yasumasa NAKA**[†], ***Student Members***, ***and*** **Masaya TAMURA**[†], ***Senior Member***

SUMMARY The load–independent zero-voltage switching class-E inverter has garnered considerable interest as an essential component in wireless power transfer systems. This inverter achieves high efficiency across a broad spectrum of load conditions by incorporating a load adjustment circuit (LAC) subsequent to the resonant filter. Nevertheless, the presence of the LAC influences the output impedance of the inverter, thereby inducing a divergence between the targeted and observed output power, even in ideal lossless simulations. Consequently, iterative adjustments to component values are required via an LC element implementation. We introduce a novel design methodology that incorporates an external quality factor on the side of the resonant filter, inclusive of the LAC. Thus, the optimized circuit achieves the intended output power without necessitating alterations in component values.

key words: *class-E inverter, resonant filter, external quality factor, wireless power transmission*

1. Introduction

In recent years, concerted efforts to advance digital transformation have intensified, motivated by factors such as a diminishing labor force and an aging population [1], [2]. Within this context, smart factories have emerged as a focal point of interest. These manufacturing facilities are distinguished by the integration of sensing technology into industrial robots, production lines, and assorted equipment, all of which are interconnected via the Internet of Things. This connectivity enables holistic data analysis and management. Smart factories confer numerous benefits, including cost minimization through the refinement of production planning and manufacturing workflows, as well as the automation of safety protocols in demanding work settings. However, challenges associated with reliability and operational efficiency persist for industrial robots, predominantly owing to issues such as cable disconnection and connector loosening, which arise from continuous operation [3], [4]. To mitigate these challenges, wireless power transfer (WPT) has been proposed as a viable solution, possessing the potential to enhance both reliability and operational efficiency by diminishing dependence on cables and connectors [5]–[14].

The WPT system designed for industrial robots consists of several key components: a high-frequency inverter, matching circuits, a wireless coupler, a rectification circuit, and the load, represented by the robot arm. The high-frequency inverter serves the critical function of converting direct current (DC) input into high-frequency (RF) output, commonly termed as DC-RF conversion. A decrement in DC-RF conversion efficiency invariably contributes to a decline in the system's overall efficiency; thus, a highly efficient inverter is desirable [15], [16]. In the MHz frequency range, both class-D and class-E inverters, which boast theoretical efficiencies approaching 100%, have captured significant attention as high-frequency power source circuits. Notably, class-E inverters employ a field-effect transistor (FET) for switching operations, obviating the need for dead-time adjustments and thereby simplifying FET drive control. In this framework, achieving high efficiency is inextricably linked to soft switching techniques, such as zero-voltage switching (ZVS) and zero-voltage differential switching (ZVDS) [17]–[19]. Class-E inverters function optimally in a soft switching mode when there is congruence between the optimal load and input impedance. Nevertheless, this soft switching mode is compromised by fluctuations in load, resulting in a consequential decrease in DC-RF conversion efficiency [20].

In WPT systems for industrial robots, the load impedance of the class-E inverter fluctuates in accordance with the operational states of the robots, such as whether they are stationary or in motion. To tackle this challenge, scholarly inquiries have been conducted into load-independent ZVS inverters with either constant voltage (CV) or constant current (CC) output functionalities [21]–[26]. Although these studies confirm the maintenance of high efficiency across a wide load spectrum, they also reveal the complexity inherent in the design methodology for control circuits. Consequently, a load-independent ZVS inverter equipped with a load adjustment circuit (LAC) has been proposed [27], [28]. The topology of LAC is influenced by both the output operating modes (CC or CV) and the optimal load, thus simplifying the design procedure. The design process for a class-E inverter involves determining application-specific design specifications and deriving component values based on these specifications. However, the introduction of the LAC alters the ratio of losses between the load-side circuit and the resonant filter, leading to a discrepancy between the targeted and measured output power. This necessitates an iterative, LC element implementation for adjusting the component values in both the inverter and LAC to achieve the target output power, even in lossless simulation scenarios.

The present paper introduces a novel design procedure for the load-independent ZVS inverter that obviates the need

Manuscript received October 27, 2023.
Manuscript revised February 8, 2024.
Manuscript publicized April 9, 2024.

[†]Department of Electrical and Electronic Information Engineering, Toyohashi University of Technology, Toyohashi-shi, 441–8580 Japan.
a) E-mail: ishiwata@comm.ee.tut.ac.jp

DOI: 10.1587/transele.2024MMP0006

for such LC element implementation by incorporating an external quality factor (Q factor). The novelty of our paper lies in the clarification and formulation of the relationship between the operating frequency and external Q factor. And it is the addition of a new design procedure to them. This external Q factor serves to indicate the ratio of losses between the load-side circuit and the resonant filter. Initially, we derive the balance between inductance and capacitance for the resonant filter, which serves as an external Q factor in the context of a load-independent class-E inverter with the LAC. Subsequently, utilizing this derived balance, an external Q factor that satisfies any predetermined output power is ascertained through circuit simulation. Following this, the resonant filter is designed based on the identified external Q factor, and simulations are executed to validate its efficacy in achieving the target output power. Ultimately, a prototyped class-E inverter equipped with an LAC demonstrates high-efficiency operation, independent of variations in load resistances.

2. Design of Load-Independent Class-E Inverter with the LAC

2.1 Conventional Method

The equivalent circuits of both the class-E inverter and the load-independent class-E inverter equipped with the LAC are depicted in Fig. 1, with the LAC being the distinguishing feature. Initially, the design methodology for the class-E inverter is outlined. The component values for this inverter can be ascertained from (1)–(5) by transforming the variables in the design formula of [19] into input conditions. In this framework, the input voltage V_{DC}, target output power P_{t}, switching frequency f_{sw}, and loaded Q factor Q_{L} serve as input conditions that vary with applications. The variables appearing in the equations express the dimensions: R_{L0} (Ω), V_{DC} (V), P_{t} (W), and f_{sw} (Hz). The series resonant elements C_{f} and L_{f} serve the role of a resonance filter, enabling only the fundamental waveform passes. L_{c} is a choke coil that allows only DC to pass through, while C_{s} is a shunt capacitor for harmonic elimination. L_0 represents a modified inductor for the soft switching. If the load resistance of the class-E inverter equals R_{L0}, both ZVS and ZVDS can be achieved simultaneously. However, achieving at least ZVS operation allows for reaching a theoretical efficiency of 100%.

$$R_{\mathrm{L0}} = \frac{8}{\pi^2+4}\frac{V_{\mathrm{DC}}^2}{P_{\mathrm{t}}} \tag{1}$$

$$C_{\mathrm{s}} = \frac{P_{\mathrm{t}}}{2\pi^2 f_{\mathrm{sw}} V_{\mathrm{DC}}^2} \tag{2}$$

$$L_{\mathrm{f}} = \frac{Q_{\mathrm{L}} R_{\mathrm{L0}} - X}{2\pi f_{\mathrm{sw}}} \tag{3}$$

$$C_{\mathrm{f}} = \frac{1}{2\pi f_{\mathrm{sw}}(Q_{\mathrm{L}} R_{\mathrm{L0}} - X)} \tag{4}$$

$$L_0 = \frac{(\pi^2-4)V_{\mathrm{DC}}^2}{4(\pi^2+4) f_{\mathrm{sw}} P_{\mathrm{t}}} \tag{5}$$

Herein, we explain the design procedure for the inverter with the LAC. In particular, LAC can presume one of eight topological configurations, which is selected based on the output modes, specifically CC or CV, and the optimal load. This research focuses on the CC output, considering the position tolerance of wireless couplers for integration into WPT systems [30], [31]. The component values for the LAC can be determined using (6)–(8) by transforming the variables in the design formula of [27] into input conditions.

$$L_1 = \frac{1}{2\pi^4 f_{\mathrm{sw}}^2 C_{\mathrm{s}}}\left(\frac{\pi^2-8}{4} + \sqrt{4\pi^2 C_{\mathrm{s}} R_{\mathrm{L0}} f_{\mathrm{sw}}}\right) \tag{6}$$

$$C_2 = \frac{1}{8 f_{\mathrm{sw}} R_{\mathrm{L0}}}\sqrt{4\pi^2 C_{\mathrm{s}} R_{\mathrm{L0}} f_{\mathrm{sw}}} \tag{7}$$

$$L_3 = \frac{2\pi}{2\pi^4 f_{\mathrm{sw}}^2 C_{\mathrm{s}}}\left(\sqrt{C_{\mathrm{s}} R_{\mathrm{L0}} f_{\mathrm{sw}}} - 2\pi f_{\mathrm{sw}} C_{\mathrm{s}} R_{\mathrm{L0}}\right) \tag{8}$$

By combining (1)–(8), a load-independent ZVS inverter can be designed to achieve ZVS operation across a wide range of load resistances.

Note that, the class-E inverter offers flexibility in balancing the resonance filter components, L_{f} and C_{f}, as indicated by (3), (4). The flexibility in this context can be represented as the load parameter Q_{L}, and its derivation is expressed in (9) using Fig. 1. ω_0 represents the resonant angular frequency. Typically, it is designed to be $\omega_0 = 2\pi f_{\mathrm{sw}}$.

$$Q_{\mathrm{L}} = \frac{\omega_0(L_0 + L_{\mathrm{f}})}{R_{\mathrm{L0}}} = \frac{1}{\omega_0 C_{\mathrm{f}} R_{\mathrm{L0}}} \tag{9}$$

In the traditional approach to class-E inverter design, (9) was utilized to configure the resonance filter. However, when dealing with a load-independent class-E inverter equipped with the LAC, the impedance of the inverter alters because of the influence of the LAC. This results in fluctuations in the ratio of losses between the LAC and the resonance filter, rendering it unfeasible to attain the target output power without the application of an LC element implementation, even in lossless simulation conditions.

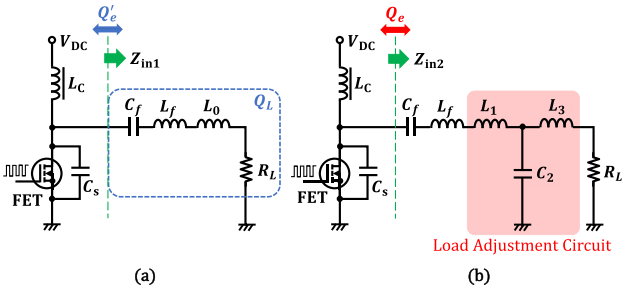

Fig. 1 Equivalent circuit diagram. (a) Class-E inverter. (b) Load-independent class-E inverter with load adjustment circuit (LAC).

2.2 Proposed Method Incorporating External Q Factor

To accurately design a class-E inverter incorporating the

LAC, we introduce a methodology that includes the external Q factor. The specifications for the load-independent class-E inverter with the LAC are uniquely determined by the input conditions. In other words, L_1, C_2, L_3, and R_L remain constant values. Additionally, the values of L_f and C_f in the resonance filter are determined by the switching frequency f_{sw}. However, the balance between L_f and C_f is flexible, and the balance is adjustable with the external Q factor.

Here, we define Q'_e and Q_e as the external Q of the simple class-E inverter and the load-independent class-E inverter, respectively. Q'_e can be determined from the input impedance Z_{in1} of the resonance filter in the simple class-E inverter. Z_{in1} can be derived by (10), which is derived from Fig. 1 (a), and Q'_e is expressd as (11) [29]. Here, assuming the resonance filter is lossless, Q_L and Q'_e are equal.

$$Z_{in1} = R + j\left\{\omega(L_0 + L_f) - \frac{1}{\omega C_f}\right\} \tag{10}$$

$$Q'_e = Q_L = \frac{\omega_0}{2}\left|\frac{\frac{d}{d\omega_0}Z_{in1}}{Z_{in1}}\right| \tag{11}$$

The relationship between the LC element of the resonance filter and Q'_e is depicted in Fig. 2. As observed, L_f is proportional to Q'_e, whereas C_f is inversely proportional. The linear approximation formula for L_f with respect to Q'_e is expressed in (12). From the relationship between the external Q factor Q'_e of the class-E inverter and the resonant filter L_f, the variable A represents the slope of L_f with respect to Q'_e variation, and B denotes the variable representing the intercept, which represents the value of L_f when $Q'_e = 0$.

$$L_f\ (\mu H) = A \cdot Q'_e - B \tag{12}$$

As A and B vary with input conditions.The input conditions are set to: $V_{DC} = 24\,V$, $P_t = 10\,W$, and $f_{sw} = 13.56\,MHz$, which is one of the industrial scientific and medical bands. These conditions imply the optimal operation, and the inverter can achieve soft switching. We varied each condition and determined the values of A and B through circuit simulation. The results are presented in Table 1. If either P_t or f_{sw} is doubled, both A and B are halved, and conversely, when they are halved, both A and B are doubled. Therefore, a reciprocal between P_t and f_{sw} is expected with respect to A and B. Similarly, when V_{DC} is doubled, both A and B increase by a factor of 2^2, and when halved, both A and B decrease by a factor of $(1/2)^2$. Therefore, a quadratic relationship exists between V_{DC} with respect to A and B. Based on the aforementioned relationships, L_f can be expressed as a variable of V_{DC}, P_t, and f_{sw} using (13).

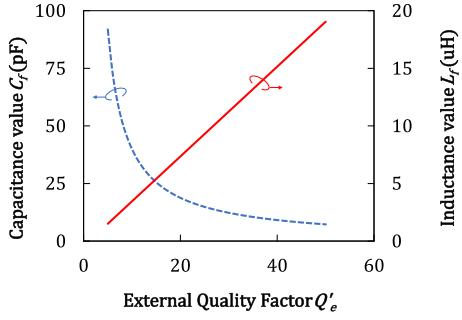

Fig. 2 Relationship between resonant filter for class-E inverter and Q'_e.

$$L_f\ (H) = \frac{V_{DC}^2}{P_t \cdot f_{sw}}(0.092Q'_e - 0.11) \tag{13}$$

C_f resonates with L_f and the operating frequency. Therefore, it can be expressed using (14).

$$C_f\ (F) = \frac{1}{L_f \cdot \omega_0^2} = \frac{P_t}{2\pi\omega_0 V_{DC}^2(0.092Q'_e - 0.11)} \tag{14}$$

From (13) and (14), the resonant filter of a standalone class-E inverter can be designed with Q'_e, regardless of the input conditions.

Furthermore, we derive the relationship between Q'_e and Q_e to design the resonant filter of the load-independent class-E with the LAC inverter. Q_e can be calculated using the input impedance Z_{in2} of the resonant filter with the LAC, as expressed in (15) and (16).

$$Z_{in2} = \frac{R_L + j\omega L_3}{1 + j\omega C_2 R_L - \omega^2 C_2 L_3} + j\left\{\omega(L_1 + L_f) - \frac{1}{\omega C_f}\right\} \tag{15}$$

$$Q_e = \frac{\omega_0}{2}\left|\frac{\frac{d}{d\omega_0}Z_{in2}}{Z_{in2}}\right| \tag{16}$$

The relationship between Q'_e and Q_e can be determined from (11), (16), and expressed as (17) which is a linear approximation, as depicted in Fig. 3.

$$Q'_e = 1.00Q_e + 0.92 \tag{17}$$

By substituting (17) into (13), L_f can be rederived using Q_e.

$$L_f\ (H) = \frac{V_{DC}^2}{P_t \cdot f_{sw}}(0.092Q_e - 0.021) \tag{18}$$

C_f resonates with L_f and the operating frequency, as expressed in (19).

$$C_f\ (F) = \frac{P_t}{2\pi\omega_0 V_{DC}^2(0.092Q_e - 0.021)} \tag{19}$$

Table 1 Variations in A and B due to varying conditions.

	Magnification	A	B
Optimal operation	× 1	0.39	0.50
V_{DC}	×0.5	0.10	0.11
	×2	1.56	1.80
P_t	×0.5	0.78	0.90
	×2	0.20	0.23
f_{sw}	×0.5	0.78	0.90
	×2	0.20	0.23

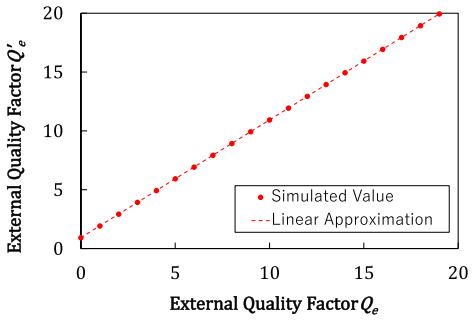

Fig. 3 Relationship between Q'_{e} and Q_{e}.

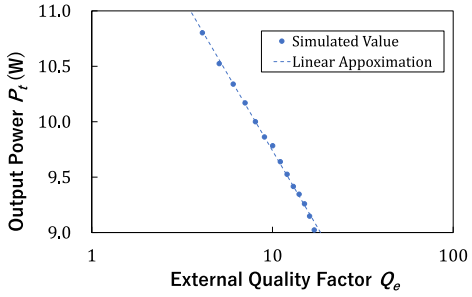

Fig. 4 Relationship between Q_{e} and P_{t} at the optimal operation of the load-independent class-E inverter with the LAC.

Table 2 Changes in C and $D - P_{\mathrm{t}}$ owing to variations in conditions.

	Magnification	C	$D - P_{\mathrm{t}}$
Optimal operation	× 1	1.18	2.48
V_{DC}	×0.5	1.19	2.48
	×2	1.17	2.49
P_{t}	×0.5	0.60	1.25
	×2	2.38	4.94
f_{sw}	×0.5	1.20	2.54
	×2	1.19	2.39

From (18) and (19), it becomes feasible to design the resonant filter for the load-independent class-E inverter with the LAC, incorporating Q_{e} regardless of the input conditions.

Finally, by implementing the redesigned resonant filter, we deduce Q_{e} through circuit simulation to achieve the target output power. Figure 4 depicts the relationship between Q_{e} and P_{t} when R_{L0} is connected. As depicted in Fig. 4, an exponential decay relationship exists between Q_{e} and the output power. Therefore, Q_{e} is expressed in (20). From the relationship between the external Q factor Q_{e} of the load-independent class-E inverter and the output power, C represents the slope of the output power with respect to Q_{e} variation, and D denotes the variable representing the intercept, which represents the output power when $Q_{\mathrm{e}} = 0$.

$$Q_{\mathrm{e}} = \exp\left(\frac{D - P_{\mathrm{t}}}{C}\right) \tag{20}$$

Variations in C and $D - P_{\mathrm{t}}$ under diverse input conditions are outlined in Table 2. Referencing Table 2 and using optimal operation as the criterion, fluctuations in V_{DC} both C and $D - P_{\mathrm{t}}$ to experience deviations of less than ±1 point. Furthermore, when P_{t} is increase to 200%, C reach 201.7%, and $D - P_{\mathrm{t}}$ reach 199.2%. When reduce to 50%, C is 50.8%, and $D - P_{\mathrm{t}}$ is 50.4%, with errors of less than ±2 points. The ±2 points error is believed to be because of the influence of component rounding errors. Thus, V_{DC} and P_{t} do not affect the formula for calculating Q_{e}. Similarly, when C is increase by 200% with respect to f_{sw}, it increase to 100.8%, and when reduce by 50%, it becomes 101.7%. The errors remained within 2 points, similar to the effect of V_{DC} and P_{t} variations. However, when $D - P_{\mathrm{t}}$ is increase by 200%, it becomes 96.4%, and when reduce by 50%, it surged to 102.4%, indicating errors larger than ±2 points. Therefore, Q_{e} is solely dependent on the frequency component. Deriving the equations for Q_{e} and frequency. Figure 5 depicts the relationship between Q_{e} and f_{sw} based on the circuit analysis results. As observed in Fig. 5, the correlation coefficient is 0.97, indicating a linear decay. The observed errors are likely because of the round-off errors in component values during circuit analysis. Using the linear approximation, the relationship between Q_{e} and f_{sw} (21).

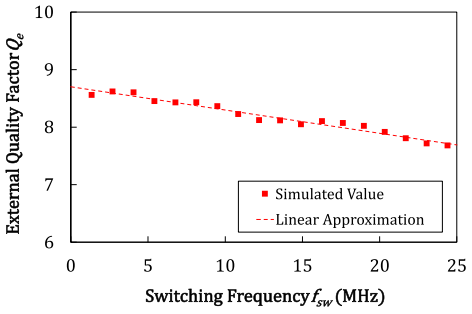

Fig. 5 Relationship between Q_{e} and f_{sw}.

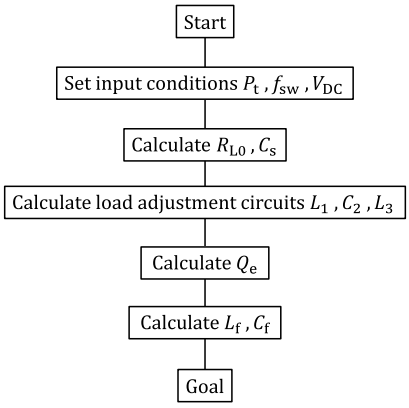

Fig. 6 Design procedure for the proposed load-independent class-E inverter with the LAC.

$$Q_{\mathrm{e}} = -4.00 \times f_{\mathrm{sw}} \times 10^{-8} + 8.70 \tag{21}$$

From (21), the target Q_{e} was set at any frequency to satisfy the target output power. Figure 6 depicts the proposed design procedure for the load-independent class-E inverter with the LAC.

3. Simulation

3.1 Single-Ended Class-E Inverter with the LAC

We employ the proposed methodology to design the load-independent class-E inverter with the LAC and assess its output power via circuit simulation. For this evaluation, a GS66502B (Gan Systems) serves as the FET in the inverter. The input conditions are specified as follows: V_{DC} = 17 V, P_t = 10 W, and f_{sw} = 13.56 MHz.

Initially, with an eye toward integration into the magnetic resonant WPT system, we conduct a single-ended analysis. To gauge the efficacy of the proposed design, the outcomes are compared by altering Q_e to 0.5 times and 2 times its obtained value. Figure 7 depicts the equivalent circuit, while Table 3 enumerates the element values employed in the circuit simulation. L_f' is the composite inductor of the resonant filter, combining the inductor L_f of the resonant filter and the inductor L_1 of the LAC. Consequently, an output power of 9.99 W with an error of 0.1% is calculated. When Q_e was reduced to 0.5 times, the output power increased to 10.33 W. Conversely, when Q_e was doubled, the output power decreased to 9.75 W. In these cases, there was a maximum deviation of up to 3.3% from the target output. In these scenarios, the maximum deviation from the target output is 3.3%, thereby improving the deviation by 3.2%. This 0.1-point error is most likely attributable to component rounding errors.

3.2 Differential Class-E Inverter with the LAC

Subsequently, considering its application within the capacitive WPT system as cited in [30], [31], a differential class-E inverter with the LAC is introduced. For the differential analysis, both Q_e and P_t settings are doubled. The LC element maintain their original values as in the single-ended configuration, and R_{L0} is doubled. Figure 8 presents the equivalent circuit. The ensuing analysis reveals an output power of 19.97 W, which corresponds to an error of 0.2% from the target value of 20 W (P_t). When Q_e is halved, the output power is 20.61 W, and when it is doubled, the output power is 19.49 W. This produces a maximum deviation of 3.1% from the target power. Thus, the deviation from the target power has improved by 2.9%. The 0.2 points error is possibly caused by component rounding errors, similar to the single-ended configuration.

Although the preceding analyses were performed under lossless conditions, it is essential to recognize that real-world inductance, capacitance, and other elements do possess losses. Accordingly, the equivalent series resistance is incorporated into the simulation. Given that the equivalent series resistance of capacitance is substantially smaller in comparison to that of inductance, only inductance loss is accounted for in the analysis. Within this framework, L_c represents a choke coil that allows only DC components to pass through, and it has multiple frequency components, rendering it challenging to calculate the losses. Therefore, we will assume it is lossless in this simulation. An unloaded Q factor of the coils is set to 300, which is realizable using toroidal coils. The analysis results display an output power of 19.13 W, which is a reduction of 4.2% compared to the lossless scenario. This decrement can largely be ascribed to inductor losses.

To further substantiate the robustness of this design against load variations, we examine both DC-RF conversion efficiency and output current. This examination assumes a specific application that achieves maximal output power when R_{L0} (optimal load) is engaged. To this end, load variations are introduced by reducing the load to 0.5 times and 0.25 times. Table 4 presents the DC-RF conversion efficiency and output current under these varying load conditions. η represents the DC-RF conversion efficiency, while I_{out} (RMS) is the root mean square value of the output power. The outcomes of the analysis confirm that the DC-RF conversion efficiency consistently remains above 90%. Moreover, the output current exhibited a maximal deviation of 2.5%, confirming stable CC output. Even when these theoretical principles are applied, the inherent advantages of a class-

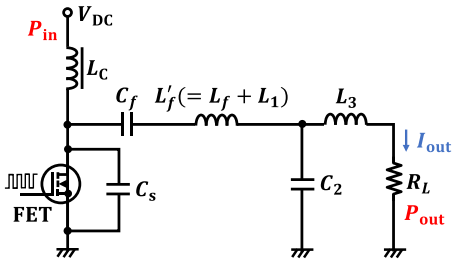

Fig. 7 Equivalent circuit of single-ended class-E inverter with the LAC.

Table 3 Element value of single-ended class-E inverter with the LAC.

	Element value		
	$0.5Q_e$	Q_e	$2.0Q_e$
L_c (μH)	4.00	4.00	4.00
C_s (pF)	42.0	42.0	42.0
C_f (pF)	183	88.7	43.7
L_f' (μH)	1.09	1.89	3.49
C_2 (pF)	594	594	594
L_3 (nH)	107	107	107
R_{L0} (Ω)	16.7	16.7	16.7

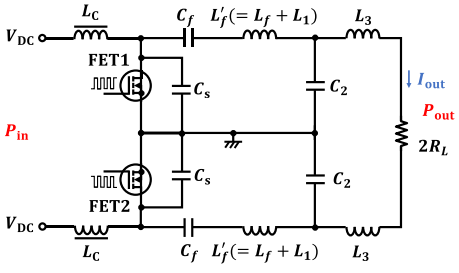

Fig. 8 Equivalent circuit of differential class-E inverter with the LAC.

Table 4 DC-RF conversion efficiency and output current under load variations.

		$0.25R_{L0}$	$0.5R_{L0}$	R_{L0}
Sim.	η (%)	93.8	95.6	95.2
	I_{out}(RMS) (mA)	776	770	757
Meas.	η (%)	87.9	90.8	89.1
	I_{out}(RMS) (mA)	786	745	720

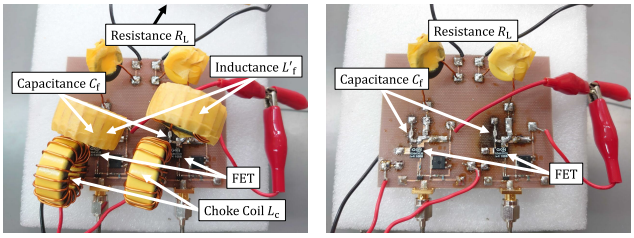

(a) Circuit layout. (b) Circuit layout with coils removed.

Fig. 9 Fabricated class-E inverter with the LAC.

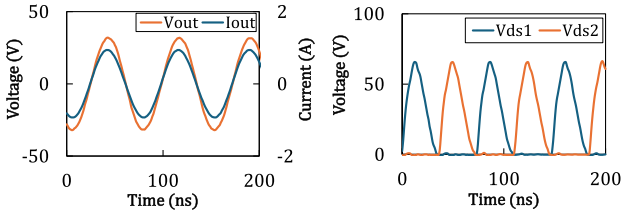

(a) Output waveform of Class-E inverter. (b) Output voltage waveform of FET.

Fig. 10 Output waveforms of the prototype class-E inverter.

Table 5 Element values of the prototype differential ZVS class-E inverter.

	Element value
L_c	3.96 , 4.00 µH
C_s	40.0 pF
C_f	111 pF
L'_f	1.56 µH
C_2	618 pF
L_3	103 nH
R_L	28.0 Ω

E inverter with the LAC namely, constant current and high efficiency are duly preserved.

4. Demonstration

We fabricated a load-independent differential class-E inverter with the LAC, as depicted in Fig. 9. The values of elements utilized in the fabrication are detailed in Table 5. Figure 10 depicts the output waveforms during class-E operation. V_{out} represents the output voltage, while V_{ds1} and V_{ds2} denote the voltage across the FETs. The outputs in Fig. 10 (a) exhibit sinusoidal waveforms, and Fig. 10 (b) confirms the ZVS operation of the FET.

However, the experimentally demonstrated output power was 14.54 W, which is notably lower than the simulated result of 19.13 W. The primary contributing factor to this discrepancy is posited to be a decrease in input power due to losses associated with the choke coil. Since the choke coil has multiple frequency components, it is challenging to calculate the losses from analysis alone. Therefore, the losses are calculated from both experimental and analytical results. Setting the unloaded Q factor of inductors other than the choke coil to 300 and calculating the losses yielded FET = 0.28 W, L'_f = 0.49 W, and L_3 = 0.04 W. Calculating the choke coil losses from the measured input/output power and these losses resulted in 0.97 W. The relationship between the target output power and external Q factor has been clarified through experimental validation. Figure 11 illustrates the relationship between the target output power and external Q factor, consistent with simulation results. As observed in both simulation and measurements, increasing the external Q factor leads to a decline in output power. Due to the inclusion of the unloaded Q factor of the coil in the measurements, the achieved target output power was not satisfactory. However, deliberately choosing a smaller external Q factor allows for a closer approximation to the target output power. Subsequently, we evaluated the DC-RF efficiency and output current across various load resistances. The optimal load resistance for the fabricated inverter was determined to be 28.0 Ω, while 7.5 Ω and 15.0 Ω were comparative resistors. As outlined in Table 4, the DC-RF conversion efficiency remained above 87%. Furthermore, with 28.0 Ω as the reference, the maximal deviation in the output current was 9.2%. Table 6 furnishes a comparative analysis between our inverter and the topologies, switch conditions, frequency, efficiency, power, output, and external Q factor. Previous studies [21]–[23] achieved load adaptability by employing two resonant filters, but this approach necessitated specialized designs tailored to each input condition, thereby escalating the design complexity. In contrast, a study [24], introduced a load-adjusting circuit to simplify the design; however, this addition led to variations in the circuit's output impedance, causing discrepancies in output power even under ideal, lossless simulations. Our paper presents a high-efficiency CC class-E inverter with the LAC that includes an external Q factor to achieve the target output without relying on an LC element implementation. This proposed methodology is advantageous for reducing man-hours in the development of WPT systems.

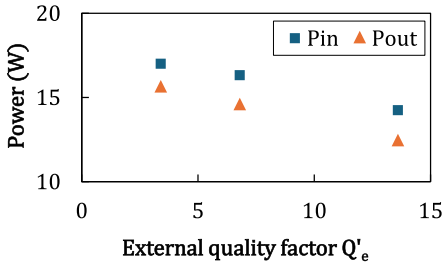

Fig. 11 Relationship between actual measured input/output power and external Q factor.

Table 6 Comparison with other research on high-frequency inverter.

	Topology	Switching condition	Frequency	Efficiency	Power	Output	External Q factor
[21]	Inverse class-E	ZCS	1 MHz	94.4%	6.96 W	CV	No
[22]	Class-E	ZVS	1 MHz	92.7%	5.75 W	CV	No
[23]	Class-E	ZVS	1 MHz	87.1%	8.30 W	CC	No
[24]	Class-E w/ LAC	ZVS	6.78 MHz	88.0%	12.6 W	CC	No
This work	Class-E w/ LAC	ZVS	13.56 MHz	89.1%	14.5 W	CC	Yes

5. Conclusion

In summary, this paper presents a design methodology that incorporates the external Q factor into a class-E inverter with the LAC to achieve the target output without utilizing an LC element implementation. Initially, a balance between inductance and capacitance for the resonant filter is derived, which subsequently serves as the external Q factor in the load-independent class-E inverter with the LAC circuit. This balanced resonant filter enables the determination of an external Q factor that meets any specific output power target through circuit analysis. In a lossless simulation scenario, the single-ended class-E inverter with the LAC yielded 9.99 W with a 0.1% error from the target 10 W output, whereas the differential class-E inverter with the LAC produced 19.97 W with a 0.2% error from the target 20 W output. These minor errors are likely attributable to component rounding errors. Furthermore, variations in the external Q factor by 0.5 times and 2 times revealed a maximum output power deviation of 3.2% in the single-ended class-E inverter with the LAC. These findings corroborate the utility of our approach when compared with existing research on high-frequency inverters, as summarized in Table 6. In summary, the differential class-E inverter with the LAC manifested a maximum deviation of 2.9% when compared with the proposed methodology. Subsequent to its fabrication, the measured output power was observed to be 14.54 W, a value lower than the simulated outcomes. The primary source of this heightened error is attributed to losses in the choke coil. The incorporation of these losses into a design methodology represents a promising avenue for future research. Additionally, we evaluated the system's resilience to load variations by adjusting the load and examining both the DC-RF conversion efficiency and output power. Consequent to these load adjustments, the DC-RF conversion efficiency consistently exceeded 87%, and the maximal deviation in output current was registered at 9.2%. These results affirm the system's high-efficiency operation and the stability of its CC output.

Acknowledgments

This work was supported by "Knowledge Hub Aichi," Priority Research Project from Aichi Prefectural Government.

References

[1] H. Tran-Dang and D.-S. Kim, "The physical Internet in the era of digital transformation: Perspectives and open issues," IEEE Access, vol.9, pp.164613–164631, Nov. 2021, doi: 10.1109/ACCESS.2021.3131562

[2] M. Baslyman, "Digital transformation from the industry perspective: Definitions, goals, conceptual model, and processes," IEEE Access, vol.10, pp.42961–42970, April 2022, doi: 10.1109/ACCESS.2022.3166937

[3] G. Tricomi, C. Scaffidi, G. Merlino, F. Longo, A. Puliafito, and S. Distefano, "A resilient fire protection system for software-defined factories," IEEE Internet Things J., vol.10, no.4, pp.3151–3164, Feb. 2023, doi: 10.1109/JIOT.2021.3127387

[4] K.-C. Chen, S.-C. Lin, J.-H. Hsiao, C.-H. Liu, A.F. Molisch, and G.P. Fettweis, "Wireless networked multirobot systems in smart factories," Proc. IEEE, vol.109, no.4, pp.468–494, April 2021, doi: 10.1109/JPROC.2020.3033753

[5] H. Kim, C. Song, D.-H. Kim, D.H. Jung, I.-M. Kim, Y.-I. Kim, J. Kim, S. Ahn, and J. Kim, "Coil design and measurements of automotive magnetic resonant wireless charging system for high-efficiency and low magnetic field leakage," IEEE Trans. Microw. Theory Tech., vol.64, no.2, pp.383–400, Feb. 2016, doi: 10.1109/TMTT.2015.2513394

[6] M.P. Kazmierkowski and A.J. Moradewicz, "Unplugged but connected: Review of contactless energy transfer systems," IEEE Ind. Electron. Mag., vol.6, no.4, pp.47–55, Dec. 2012, doi: 10.1109/MIE.2012.2220869

[7] T. Fujita, T. Yasuda, and H. Akagi, "A dynamic wireless power transfer system applicable to a stationary system," IEEE Trans. Ind. Appl., vol.53, no.4, pp.3748–3757, July 2017, doi: 10.1109/TIA.2017.2680400

[8] R. Trevisan and A. Costanzo, "A 1-kW contactless energy transfer system based on a rotary transformer for sealing rollers," IEEE Trans. Ind. Electron., vol.61, no.11, pp.6337–6345, Nov. 2014, doi: 10.1109/TIE.2014.2311395

[9] R. Trevisan and A. Costanzo, "A UHF near-field link for passive sensing in industrial wireless power transfer systems," IEEE Trans. Microw. Theory Tech., vol.64, no.5, pp.1634–1643, May 2016, doi: 10.1109/TMTT.2016.2544317

[10] X. Wu, S. Chen, J. Li, X. Li, W. Gong, and Z. Wang, "A parallel transmission method of power and data in WPT system based on data transmission of single capacitor plate," 2022 IEEE 9th Int. Conf. Power Electron. Syst. Appl. (PESA), pp.1–4, Hong Kong, Sept. 2022, doi: 10.1109/PESA55501.2022.10038353

[11] Y. Mo, S. Wu, X. Li, J. Xiao, S. Chen, and Z. Wang, "Research on simultaneous wireless power and data transfer system based on ASK modulation," 2022 IEEE 9th Int. Conf. Power Electron. Syst. Appl. (PESA), pp.1–5, Hong Kong, Sept. 2022, doi: 10.1109/PESA55501.2022.10038375

[12] N. Ashraf, S.A. Sheikh, S.A. Khan, I. Shayea, and M. Jalal, "Simultaneous wireless information and power transfer with cooperative relaying for next-generation wireless networks: A review," IEEE Access, vol.9, pp.71482–71504, May 2021, doi: 10.1109/ACCESS.2021.3078703

[13] B. Clerckx, R. Zhang, R. Schober, D.W.K. Ng, D.I. Kim, and H.V. Poor, "Fundamentals of wireless information and power transfer: From RF energy harvester models to signal and system designs," IEEE J. Sel. Areas Commun., vol.37, no.1, pp.4–33, Jan. 2019, doi: 10.1109/JSAC.2018.2872615

[14] J. Wu, K. Feng, N. Jin, Y. Liang, J. Zhang, C.C. Yao, and J. Tao, "A simultaneous wireless information and power transfer system with independent channel for information transfer," IEEE Access, vol.8, pp.125610–125619, July 2020, doi: 10.1109/ACCESS.2020.3007888

[15] K. Peng and E. Santi, "Class E resonant inverter optimized design for high frequency (MHz) operation using eGaN HEMTs," 2015 IEEE Appl. Power Electron. Conf. Expo. (APEC), pp.2469–2473, Charlotte, NC, USA, March 2015, doi: 10.1109/APEC.2015.7104695

[16] S. Koyama, M. Mizutani, and T. Ohira, "Power imbalance compensation of parallel combining twin class-E inverters by DC current detection fed back to gate-signal phase control," 2020 IEEE Int. Conf. Power Energy (PECon), pp.89–94, Penang, Malaysia, Dec. 2020, doi: 10.1109/PECon48942.2020.9314592

[17] N.O. Sokal and A.D. Sokal, "Class E—A new class of high-efficiency tuned single-ended switching power amplifiers," IEEE J. Solid-State Circuits, vol.10, no.3, pp.168–176, June 1975, doi: 10.1109/JSSC.1975.1050582

[18] F. Raab, "Idealized operation of the class E tuned power amplifier," IEEE Trans. Circuits Syst., vol.24, no.12, pp.725–735, Dec. 1977, doi: 10.1109/TCS.1977.1084296

[19] T. Suetsugu and M. Kazimierczuk, "Steady-state behavior of class E amplifier outside designed conditions," IEEE Int. Symp. Circuits Syst., vol.1, pp.708–711, Kobe, Japan, May 2005, doi: 10.1109/ISCAS.2005.1464686

[20] T. Ohira, "Load impedance perturbation formulas for class-E power amplifiers," IEICE Commun. Exp., vol.9, no.10, pp.482–488, Oct. 2020, doi: 10.1587/comex.2020XBL0085

[21] A. Komanaka, W. Zhu, X. Wei, K. Nguyen, and H. Sekiya, "Generalized analysis of load-independent ZCS parallel-resonant inverter," IEEE Trans. Ind. Electron., vol.69, no.1, pp.347–356, Jan. 2022, doi: 10.1109/TIE.2021.3053888

[22] N. Obinata, W. Luo, X. Wei, and H. Sekiya, "Analysis of load-independent class-E inverter at any duty ratio," IECON 2019 - 45th Annu. Conf. IEEE Ind. Electron. Soc., pp.1615–1620, Lisbon, Portugal, Oct. 2019, doi: 10.1109/IECON.2019.8927599

[23] T. Sensui and H. Koizumi, "Load-independent class E zero-voltage-switching parallel resonant inverter," IEEE Trans. Power Electron., vol.36, no.11, pp.12805–12818, Nov. 2021, doi: 10.1109/TPEL.2021.3077077

[24] L. Zhang and K. Ngo, "A constant current ZVS class-E inverter with finite input inductance," IEEE Trans. Ind. Electron., vol.68, no.8, pp.7693–7696, Aug. 2021, doi: 10.1109/TIE.2020.2998764.

[25] L. Roslaniec, A.S. Jurkov, A.A. Bastami, and D.J. Perreault, "Design of single-switch inverters for variable resistance/load modulation operation," IEEE Trans. Power Electron., vol.30, no.6, pp.3200–3214, June 2015, doi: 10.1109/TPEL.2014.2331494

[26] H. Sekiya, K. Tokano, W. Zhu, Y. Komiyama, and K. Nguyen, "Design procedure of load-independent class-E WPT systems and its application in robot arm," IEEE Trans. Ind. Electron., vol.70, no.10, pp.10014–10023, Oct. 2023, doi: 10.1109/TIE.2022.3220818

[27] M. Mizutani, S. Koyama, S. Abe, and T. Ohira, "Geodesic theory of zero-voltage-switching RF power inverters for constant-voltage or -current output operation," 2020 IEEE Int. Conf. Power Energy (PECon), pp.83–88, Penang, Malaysia, Dec. 2020, doi: 10.1109/PECon48942.2020.9314539

[28] S. Liu, M. Liu, M. Fu, C. Ma, and X. Zhu, "A high-efficiency class-E power amplifier with wide-range load in WPT systems," 2015 IEEE Wireless Power Transfer Conf. (WPTC), pp.1–3, Boulder, CO, USA, May 2015, doi: 10.1109/WPT.2015.7140140

[29] T. Ohira and T. Wuren, "Pseudolinear circuit theory for sinusoidal oscillator performance maximization," IEICE Trans. Electron., vol.E91-C, no.11, pp.1726–1737, Nov. 2008, doi: 10.1093/ietele/e91-c.11.1726

[30] Y. Naka, A. Ishiwata, and M. Tamura, "Capacitive wireless power transfer independent of load impedance fluctuation with transfer distance," 2023 IEEE/MTT-S Int. Microw. Symp., pp.883–886, San Diego, CA, USA, June 2023, doi: 10.1109/IMS37964.2023.10188100

[31] Y. Naka, A. Ishiwata, and M. Tamura, "Capacitive wireless power transfer system with misalignment tolerance in flowing freshwater environments," IEICE Trans. Electron., vol.E107-C, no.2, pp.47–56, Feb. 2024, doi: 10.1587/transele.2023ECP5018

Akihiko Ishiwata received the B.E. degree in electrical and electronic information engineering from Toyohashi University of Technology (TUT), Toyohashi, Japan, in 2022. His current research interests include RF inverter and wireless power transfer.

Yasumasa Naka received the B.E. and M.E. degrees in electrical and electronic information engineering from Toyohashi University of Technology (TUT), Toyohashi, Japan, in 2016 and 2018, respectively. From 2018 to 2020, he was with NIDEK CO., LTD. where he was engaged in the development of a wireless power transfer and wireless communication device for use in retinal prosthesis. From 2020 to 2021, he was associated with the Research Center for Future Vehicle City with TUT. He is currently pursuing a Ph.D. degree in electrical and electronic information engineering at TUT. His current research interests include wireless power transfer and dielectrics. He is a JSPS research fellow (DC2).

Masaya Tamura received the B.E. and M.E. degrees from Okayama University, Okayama, Japan in 2001 and 2003, respectively, and the Ph.D. degree from Kyoto University, Kyoto, Japan in 2012. From April 2003 to March 2014, he has worked at Panasonic Co. Ltd., where he has been engaged in research and development on high-frequency components including lightwave, especially microwave filters, metamaterials, and plasmonics. In April 2014, he joined the Toyohashi University of Technology, where he is currently a Professor of Electrical and Electronic Information Engineering. His current research interests include microwave circuits and wireless power transfer. Dr. Tamura was the recipient of the IEEE MTT-S Outstanding Young Engineer Award in 2015. He has also received the 2012 IEEE MTT-S Japan Young Engineer Award and the 2012 Michiyuki Uenohara Memorial Award.